Measurement and multiple-scattering calculation of Cu *K*-edge x-ray magnetic circular dichroism spectra from an exchange-coupled Co/Cu multilayer

S. Nagamatsu, H. Matsumoto, and T. Fujikawa
Graduate School for Science, Chiba University, Yayoi, Inage, Chiba 263-8522, Japan

K. Ishiji and H. Hashizume*
Research and Education Center for Materials Science, Nara Institute of Science and Technology, Takayama, Ikoma 630-0192, Japan
(Received 29 July 2004; revised manuscript received 27 August 2004; published 19 November 2004)

Small but significant x-ray magnetic circular dichroic (XMCD) absorptions are observed from an exchange-coupled Co/Cu multilayer at the Cu *K* edge. Multiple-scattering calculations including the spin-orbit interaction show that the Cu dichroism is almost entirely due to the spin-dependent scattering of photoelectrons by the exchange potentials of Co atoms at the interface. Possible small magnetic moments induced on Cu account for a marginal fraction of the observed Cu dichroism. The calculated XMCD spectra are highly sensitive to the local magnetic structure around the x-ray absorbing site. Layer-resolved magnetic absorption spectra calculated near the *K* edge of Cu demonstrate that the core excitation on the interface layer dominates the mean XMCD spectrum from the Cu film. Discussion is extended on the effect of interface roughness and the determination of the spin asymmetry of delocalized electrons in Cu layers in the context of the exchange coupling of Co/Cu.

DOI: 10.1103/PhysRevB.70.174442 PACS number(s): 75.70.Cn, 78.20.Ls, 11.80.La, 71.70.Gm

I. INTRODUCTION

Spin polarizations of delocalized electrons in nonmagnetic spacer layers play an essential role in the indirect exchange coupling of magnetic/nonmagnetic metal multilayers.[1,2] Among various exchange-coupled metal systems known to date,[3] Co/Cu has been the most extensively investigated for two reasons. On the experimental side, the small lattice mismatch between Co and Cu, along with the immiscibility of the two elements, allows high-quality samples to be grown with sharp interfaces.[4–6] On the theoretical side, noble metal Cu has a simple band structure with an accurately known Fermi surface via de Haas–van Alphen measurements. In this system, nearly free electrons in Cu become spin polarized through magnetic interactions with the Co layer at the interface. The polarization propagates across the Cu layer and interacts with another Co layer, thereby giving rise to a magnetic coupling between the Co moments.[1] The Cu electrons form quantum-well states with discrete densities of states near the Fermi level, which were proven to be of minority character.[2,7–9] Photoemission measurements confirmed as well that the oscillatory exchange couplings in Co/Cu(100) as a function of the Cu-layer thickness are dictated by the topology of the Cu Fermi surface.[10–14]

Further evidence for the spin-polarized Cu electrons in Co/Cu multilayers is provided by x-ray magnetic circular dichroism (XMCD) measurements.[15,16] The similar XMCD spectra observed at the Co and Cu *K* edges suggest that the conduction bands of Cu are magnetically polarized via 4*p*-3*d* hybridization at the Cu/Co interface.[16] In addition, the same polarity of the Co and Cu signals observed indicates that the 4*p* moments of Cu ($\sim -0.02\mu_B$) are aligned parallel to the Co 4*p* ($\sim -0.05\mu_B$) moment. Interestingly, the Cu XMCD signals decay more slowly than the $1/t_{Cu}$ law in a series of sputtered Co(1.2 nm)/Cu(t_{Cu}) samples with t_{Cu} ranging from 0.4 to 2.0 nm.[16] This suggests that the induced polarization is extended beyond the interface area into the interior of the Cu layer, in accordance with the quantum-interference picture.[1] By contrast, the polarization of Cu 3*d* electrons has a dominant interfacial nature, as seen in a dichroism measurement at the *L* edge.[15] The observed Cu moments are parallel to those of Co, which are nearly identical in magnitude to bulk Co, independent of Cu thickness. The spin moment in the Cu *d* shell is $0.013\mu_B$ in a Co(1.0 nm)/Cu(1.3 nm) multilayer. The Cu $L_{2,3}$ x-ray absorption near-edge structure (XANES) spectra show an increase in the white-line intensity with decreasing Cu thickness, suggesting an increased number of *d* holes in Cu atoms near the interface. The conclusion is intriguing, but the discussion is based on the atomic picture.

Our recent works on amorphous Gd-Co alloys[17] and Fe-*M* (*M*=Al, Sn) spin glass[18,19] clearly show that the *K*-edge XMCD is significantly affected by the local structures around the x-ray absorbing atoms, both chemical and magnetic. This motivated us to obtain a deeper insight into the spin polarization of delocalized Cu electrons in Co/Cu multilayers by analyzing the XMCD data with the use of the fully relativistic multiple-scattering approach.[20,21] In this paper, we will show that Cu *K*-edge XMCD signals do not represent true magnetic moments on Cu, but are dominated by the spin-dependent scattering of delocalized electrons by interface Co atoms. The paper begins with outlining the multiple-scattering formalism in Sec. II. This is followed by a description of an experiment to measure high-resolution XMCD spectra in Sec. III. The models and assumptions used to simulate the data by multiple-scattering calculations are presented in Sec. IV. The results are compared with the experiment in Sec. IV, where we discuss the effects of magnetic moments on Cu atoms and interface roughness. In Sec. V we refer to the determination of the spin asymmetry of delocalized Cu electrons in the context of the indirect exchange coupling.

II. MULTIPLE-SCATTERING THEORY

We outline here the multiple-scattering formalism presented in Refs. 20 and 21. As in XANES spectra, the multiple scatterings play an important role in XMCD spectra in near-edge regions. If we neglect the spin-flip scatterings at the nearby atoms,[20,22–24] the multiple scattering is written as

$$T^{(\infty)} = T^{(0)} + T^{(1)} + T^{(2)} + \cdots, \tag{1}$$

where $T^{(0)}$, $T^{(1)}$, and $T^{(2)}$ are the atomic-, single-, and double-scattering terms, respectively. These are derived from $T(m_p, m_p')$ defined in terms of core function $|c\rangle$ and full Green's function g describing the photoelectron propagation with energy ε,

$$T(m_p, m_p') = -2\,\mathrm{Im}\langle c|\Delta_{m_p}^{*} g(\varepsilon)\Delta_{m_p'}|c\rangle, \tag{2}$$

where m_p and m_p' stand for the photon helicity $(-1, 0, +1)$. The electron-photon interaction operator Δ_{m_p} is given by $\Delta_{m_p} = rY_{1m_p}(\hat{\mathbf{r}})$, neglecting unimportant constants. We have an explicit expression of XMCD for single crystals[20,21]

$$\Delta T \cos\beta + \frac{\delta T}{\sqrt{2}} \sin\beta. \tag{3}$$

Here the magnetic field is along the z direction and the incident x-ray photons arrive on the target from the positive z' direction; $\mathbf{e}_{z'} \cdot \mathbf{e}_z = \cos\beta$. For the K-edge XMCD the renormalized full multiple-scattering series are given by the compact formula shown below:

$$\Delta T = \Delta T^0 - \frac{4}{\pi}\,\mathrm{Im}[\rho_1^{+}(k^{+})_c \delta\rho_1^{+}(k^{+})_c \exp(2i\delta_1^{A+})(Z^{+})_{11,11}^{A,A} - (+\,\mathrm{spin} \rightarrow -\,\mathrm{spin})], \tag{4}$$

$$\delta T = \delta T^0 - \frac{4}{\pi}\,\mathrm{Im}[\rho_1^{+}(k^{+})_c \delta\rho_1^{+}(k^{+})_c \exp(2i\delta_1^{A+})\{(Z^{+})_{11,10}^{A,A} - (Z^{+})_{1-1,10}^{A,A}\} - (+\,\mathrm{spin} \rightarrow -\,\mathrm{spin})], \tag{5}$$

where $(+\mathrm{spin} \rightarrow -\mathrm{spin})$ means the same term as the first term with the up $(+)$ spin interchanged by the down $(-)$ spin. In Eqs. (4) and (5), radial dipole integral ρ_l between the core function and the lth partial wave weakly depends on the photoelectron energy. This is also the case with $\delta\rho_l$, which includes the spin-orbit interaction. We have used

$$Z^{\pm} = G(1 - X^{\pm})^{-1}, \tag{6}$$

$$(X^{\pm})_{LL'}^{\alpha\beta} = t_l^{\alpha\pm}(k^{\pm}) G_{LL'}(\mathbf{R}_\alpha - \mathbf{R}_\beta). \tag{7}$$

In Eqs. (6) and (7) the free propagators in the angular momentum representation $G_{LL'}$ reflect the geometrical structure, whereas the site T matrix $t_l^{\alpha\pm}$ reflects the electronic and magnetic structures of site α. The renormalized matrix Z describes the spin-dependent full multiple scatterings of photoelectrons inside the cluster. The atomic terms, ΔT^0 and δT^0 in Eqs. (4) and (5), vanish when spin-orbit coupling is negligible or the spin polarization is small enough on the x-ray absorbing atom. We may rewrite the dichroism given by Eq. (3) as

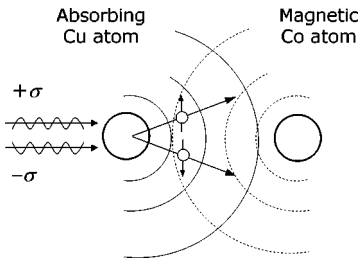

FIG. 1. A Cu atom absorbs circularly polarized x-ray photons of helicities $+\sigma$ and $-\sigma$. Ejected spin-polarized photoelectrons travel to nearby Co atoms and are spin-dependently scattered. The outgoing and backscattered photoelectron waves interfere to affect helicity-dependent x-ray absorption rates on the absorber.

$$\Delta\mu_a + \Delta\mu_n, \tag{8}$$

where $\Delta\mu_a$ is the atomic contribution arising from the first terms of Eqs. (4) and (5), whereas $\Delta\mu_n$ is the contribution from the second terms of these equations, representing the dichroism due to the multiple scattering of photoelectrons. We make it clear that $\Delta\mu_a$ corresponds to σ_{1a} defined by Rueff *et al.*,[25] while $\Delta\mu_n$ does to $\sigma_{1l} + \sigma_{1n}$. Note that $\Delta\mu_n$ originates from the spin-dependent scattering of photoelectrons by magnetic neighbors. It gives rise to a finite dichroism even when the x-ray absorbing atom is nonmagnetic. Photoelectrons ejected from absorbing Cu atoms travel to nearby Co atoms and are spin-dependently scattered.[26] The interference of the outgoing and back-scattered photoelectron waves influences the helicity-dependent x-ray absorption rates on the absorbing Cu atoms (Fig. 1).

III. EXPERIMENT

A. Sample growth and characterization

The multilayer investigated in this work has 50 bilayers of Co(1.24 nm)/Cu(1.77 nm), grown on polyimide films with a 5-nm-thick Ta buffer layer at room temperature by magnetron sputter deposition in a high-vacuum chamber. The growth rates are 0.32 nm s^{-1} for Co and 0.25 nm s^{-1} for Cu at an argon pressure of 4×10^{-1} Pa. We finished the deposition by capping the top Co surface with a 1.8-nm-thick Cu layer. The same multilayer was grown on silicon substrates, in the same deposition run as the XMCD sample, for x-ray diffraction and magnetic measurements. The silicon wafers were mirror-polished but not chemically etched; the multilayers were grown on surface oxides. An x-ray reflectometry trace fitted to Parratt's formula[27] showed the layer thicknesses indicated above and a root-mean-squares roughness of 0.45 nm at the Co/Cu interface, which is reasonably small for a sputtered film. Wide-angle x-ray diffractometer scans showed no well-defined peak, indicating a poor crystalline quality of the sample. The sample showed an in-plane peak magnetoresistance ratio, MR, of 20.4% at room temperature, where MR is defined by $(R - R_{\mathrm{sat}})/R_{\mathrm{sat}}$ with R_{sat} being the electrical resistance at a saturation field. This is close to ~25% reported for similar Co/Cu multilayers.[4]

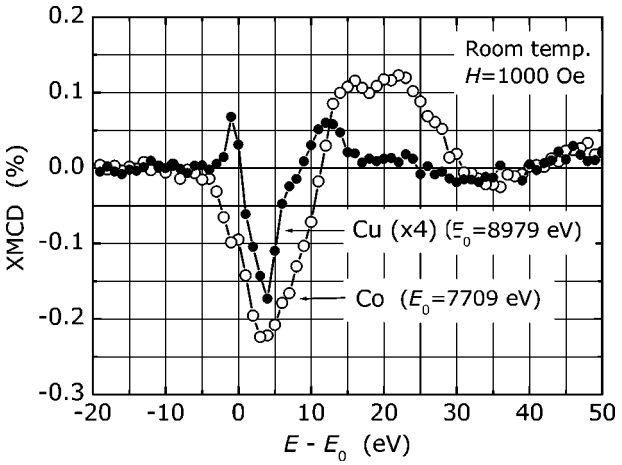

FIG. 2. Co and Cu *K*-edge XMCD spectra observed from a $[\mathrm{Co}(1.24\ \mathrm{nm})/\mathrm{Cu}(1.77\ \mathrm{nm})]_{50}$ multilayer at room temperature. A saturating in-plane field of 1000 Oe was applied along the projected wave vector of circularly polarized probing x rays. Note the Cu spectrum multiplied by 4. E_0 indicates the absorption-edge energy.

B. XMCD measurement

We collected XMCD data for the Co and Cu *K* edges at station BL39XU in SPring-8, Japan Synchrotron Radiation Research Institute, using the helicity modulation lock-in technique.[28,29] This employed a 0.45-mm-thick (111) diamond quarter-wavelength phase plate, rotary oscillated between the two predetermined angular positions across the $\bar{2}20$ Bragg position with a frequency of 30 Hz. The degree of circular polarization of the transmitted beam is estimated to be higher than 90%. The circularly polarized x-ray beam of alternating helicity was led on to a sample at a 45° glancing angle. An external in-plane field of 1000 Oe was applied along the projection of the x-ray wave vector on to the sample plane. This field is sufficiently high to align the Co moments along the field. We measured XMCD in the transmission geometry. The output signals of two ion chambers, placed before and after the sample, were fed into logarithmic converters followed by a lock-in amplifier for a phase-sensitive measurement of magnetic and nonmagnetic absorption signals.[28,29] The setup allowed us to acquire a Cu *K*-edge XMCD spectrum of high signal-to-noise ratio in 30 min at a resolution of 1 eV. The data collection time was even shorter at the Co *K* edge. The measurement was repeated with reversed magnetic fields to remove nonmagnetic dichroisms from the data.

Figure 2 shows XMCD spectra observed at the *K* edges of Co and Cu. We define here XMCD by $\Delta\mu/\mu_{\mathrm{jump}}=[\mu(-,+)-\mu(+,+)]/\mu_{\mathrm{jump}}$ or $\Delta\mu/\mu_{\mathrm{jump}}=[\mu(+,-)-\mu(-,-)]/\mu_{\mathrm{jump}}$, where μ is the absorption coefficient. The signs in the first and second positions in the parentheses stand for the photon helicity and the field direction, respectively. We define the + field along the projected x-ray **k** vector. μ_{jump} is the jump height of μ at the absorption edge. This widely used definition is opposite to the one we have used in our resonant x-ray magnetic scattering works.[30–33] The observed dichroic spectra mimic the previously reported ones[16] for both Co and Cu, though more structures are resolved in Fig. 2. The Co dichroism presents a main peak at 4 eV above the absorption edge ($E_0=7709$ eV), accompanied by a smaller but broader truncated peak, opposite in sign, occupying an energy range of $10\leqslant E-E_0\leqslant 30$ eV. This spectrum looks very similar to the one from hcp Co metal.[25] The Cu dichroism is much weaker, with a main peak about one-fifth as large as the Co peak, located at 4 eV above the absorption edge ($E_0=8979$ eV). It reaches 0.055% when we correct for the 45° angle that the in-plane magnetization vector makes to the **k** vector of the probing x rays ($\beta=45°$). The general profile follows the one for Co as observed by Pizzini *et al.*,[16] though markedly narrower in energy spread. This is clearly seen in Fig. 2. The small prepeak at $E\approx E_0$, characteristic of the Cu spectrum, is more enhanced than previously observed.[16] Note that the Cu spectrum shows a valley-peak structure of the same polarity as the Co spectrum, although the positive prepeak is missing in Co. This indicates that the Cu 4*p* band is spin polarized with a spin asymmetry of the same sign as that of the Co 4*p* band.

We should note that *K*-edge XMCD is observed when the following two conditions are simultaneously met: (1) the spin-orbit interaction on the x-ray absorbing atom influences the final-state symmetry of the photoelectron wave function, and (2) the spin polarizations of nearby atoms discriminate the spin-dependent scattering of photoelectrons due to the exchange scattering. The finite Cu *K*-edge XMCD observed in Fig. 2 does not necessarily indicate magnetic moments on Cu atoms, as pointed out in Sec. II.

IV. SIMULATION CALCULATION AND DATA ANALYSIS

A. Models and assumptions

To simulate the data using the multiple-scattering formalism outlined in Sec. II, we model our Co/Cu multilayer with a (100) superlattice of Co(7 AL)/Cu(10 AL), where AL stands for atomic layers. For comparison, we investigate a (111) superlattice of Co(6 AL)/Cu(8 AL) as well. In both models, fcc Co is assumed to have the same lattice constant as bulk Cu (0.362 nm). To estimate the electron configurations on the Co and Cu sites, we started from the electron numbers given by the code[34] FEFF8 for the 3*d* and 4*s*+4*p* states of bulk Co and Cu. These numbers are listed in Table I for Co(2)-Co(4) and Cu(2)-Cu(5) in the Co/Cu(100) model. Co atoms at the interface tend to acquire *d* electrons from Cu because of the hybridization, as indicated by Zahn *et al.*[35] We transferred a 3*d* charge from Cu(1) to Co(1) by trial and error, while retaining the 4*s*+4*p* charge, and determined an optimal 3*d* charge transfer to reproduce the observed *K*-edge XANES and XMCD spectra shown in Figs. 2 and 3. A variation in the 3*d* electron number modifies the scattering potentials of Co and Cu, which results in a shift of the calculated spectra. This procedure revealed 0.4 3*d* electrons moved from Cu(1) to Co(1). Note in Table I that our model assumes modified electron configurations only on the interface layers. For the magnetic moments, we quote the values given by Samant *et al.*[15] for Co [see Table I and Fig. 2(c) in Ref. 15] and assume no moment induced on Cu. We apply the electron and magnetic moment configuration of Table I to the Co/Cu(111) model as well.

TABLE I. Charge and magnetic-moment configurations for the fcc Co(7)/Cu(10) model. The (100) layers are numbered according to the distance from the interface.

	Electron number		Magnetic moment in μ_B	
Layers	$3d$	$4s+4p$	$3d$	$4s+4p$
Cu(5)	9.70	1.30	0	0
Cu(4)	9.70	1.30	0	0
Cu(3)	9.70	1.30	0	0
Cu(2)	9.70	1.30	0	0
Cu(1)	9.30	1.30	0	0
Co(1)	8.25	1.15	1.65	−0.07
Co(2)	7.85	1.15	1.65	−0.07
Co(3)	7.85	1.15	1.65	−0.07
Co(4)	7.85	1.15	1.65	−0.07

In the calculation of crystal potentials, we chose the muffin-tin radius of Co and Cu at 0.128 nm and spherically averaged the potential at each atom site. All interstitial sites were assumed to have a constant potential, E_i. We estimated the scattering phase shifts for photoelectrons using the conventional nonlocal Hartree-Fock method and carried out multiple-scattering calculations for clusters of ~135 atoms. Good convergence was achieved for smooth and rough interface models. To make the onsets and peaks of the calculated XANES spectra coincide with those observed, we suppressed absorptions related to photoelectrons of energies less than E_i+10 eV in Co and E_i+9 eV in Cu. Absorptions occur when core electrons are excited to unoccupied states above the Fermi level. We thus placed the calculated spectra on the energy scale of the experiment. The calculated XMCD spectra were then cutoff at E_i+10 eV in Co and E_i+9 eV in Cu. To account for the effect of the finite core-hole lifetime, we convoluted the calculated XANES and XMCD spectra with a Lorentzian of 1.4 eV in full width at half maxima, assuming an equal lifetime for Co and Cu. This value is close to the mean of 1.33 and 1.55 eV, tabulated for Co and Cu, respectively, by Krause and Oliver.[36] The layer-by-layer XANES spectra thus calculated were averaged. The mean spectra for Co and Cu were individually scaled to the jump heights μ_{jump} of the experimental absorption curves observed at the respective K edges.

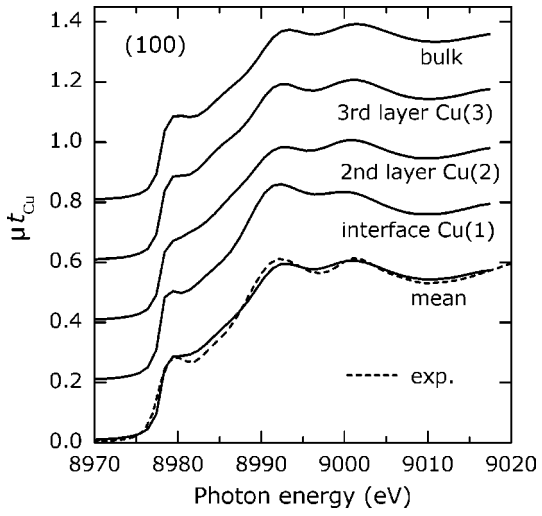

FIG. 3. Layer-resolved K-edge XANES spectra calculated for layers Cu(1), Cu(2), and Cu(3) in a Co(7 AL)/Cu(10 AL) model with the (100) interface (full line). The "mean" spectrum is a sum of contributions from Cu(1)-Cu(10) divided by 10. The "bulk" spectrum is calculated for bulk Cu crystal. The broken line shows the experimental absorption spectrum.

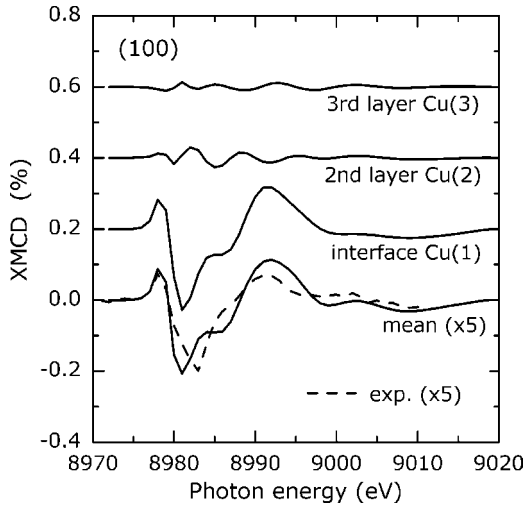

FIG. 4. Layer-resolved Cu K-edge XMCD spectra for the interface, second, and third Cu layers in the Co/Cu(100) model (full line). The mean spectrum is a sum of contributions from the ten Cu layers divided by 10. The broken line indicates the experimental spectrum of Fig. 2 corrected for the x-ray incidence angle. The mean and experimental spectra are multiplied by 5.

B. Multiple-scattering calculations

Figure 3 shows the calculated layer-by-layer XANES spectra for the Co/Cu(100) model at the Cu K edge, where the mean spectrum is shown along with the experimental one. The interface spectrum for Cu(1) is featured by an enhanced peak at ~8980 eV. The peak becomes lower and broader on the second and third layers, Cu(2) and Cu(3), with the global profile approaching the spectrum calculated for bulk Cu crystal. The mean XANES spectrum, which slightly differs from the bulk spectrum, follows the observation closely. The corresponding XMCD spectra are shown in Fig. 4. Note that a large dichroism is observed only on Cu(1), which is totally due to the scattering term $\Delta\mu_n$ in Eq. (8) since there is no magnetic moment assumed on Cu, i.e., $\Delta\mu_a=0$. The finite dichroisms observed on Cu(2) and Cu(3) indicate that photoelectrons pick up magnetic information from Co atoms located in the second- and third-neighbor sites. These make small contributions to the total XMCD from the Cu film. Note that the mean spectrum, which is the sum of the contributions from the ten Cu layers divided by 10, agrees with the experimental spectrum not only in magnitude but also in profile, even though some discrepancy is seen on the high-energy flank of the main peak.

The Cu K-edge XANES spectra calculated for the (111) interface model turned out to be very similar to those in Fig.

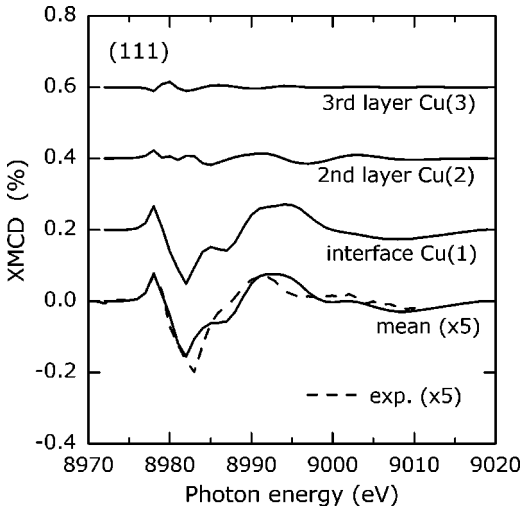

FIG. 5. Same as Fig. 4 but for the Co/Cu(111) model.

3. Figure 5 shows the layer-resolved dichroism spectra for this model. The contribution from the interface layer Cu(1) is slightly smaller than in the (100) model, but still dominates the mean XMCD spectrum. Again, the agreement of the mean spectrum with the experiment is good, though not perfect. A comparison with Fig. 4 shows that it is hard to judge which of the two models better reproduces the observed XMCD spectrum.

Comparing the XMCD strengths measured at the Co and Cu *K* edges, Pizzini *et al.* estimates $-0.02\mu_B$ for the $4p$ moment on copper in their Co(1.2 nm)/Cu(0.8 nm) multilayer.[16] To investigate the contribution that a Cu moment can make to the total dichroism, we calculated the mean XMCD spectrum from the ten Cu layers in our Co/Cu(100) model with a $4s+4p$ moment of $-0.02\mu_B$ given to all Cu atoms. Namely, we replaced 0 entered for $4s+4p$ in Table I by −0.02 with the other parameters unchanged. The result is shown in Fig. 6, where the Cu moment produces a significant dichroism due to the $\Delta\mu_a$ term [Eq. (8)], which is no longer zero. While this demonstrates an excellent sensitivity of XMCD to a small moment, we point out that the

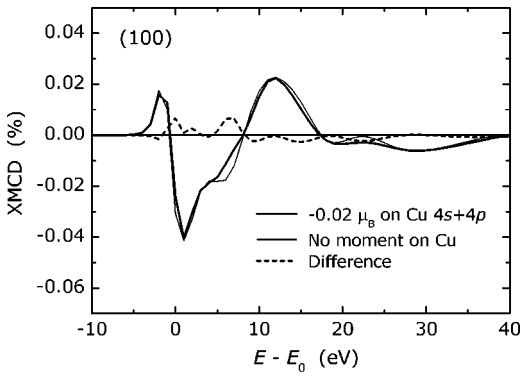

FIG. 6. Mean Cu *K*-edge XMCD spectra for the Co/Cu(100) model with a magnetic moment of $-0.02\mu_B$ (thick line) and $0\mu_B$ (thin line) given to the $4s+4p$ state of all Cu atoms. The dotted line shows the difference of the two spectra, representing the contribution from $-0.02\mu_B$.

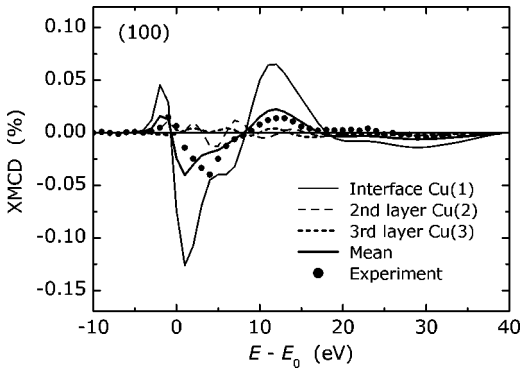

FIG. 7. Layer-resolved Cu *K*-edge XMCD spectra for the Co/Cu(100) model with a $-0.02\mu_B$, magnetic moment given to the $4s+4p$ state of all Cu atoms. Dots trace the experimental spectrum for comparison.

$\Delta\mu_a$ contribution occupies a small fraction of the total Cu *K*-edge dichroism, which is dominated by the $\Delta\mu_n$ contribution, as can be seen from the closely spaced thick and thin lines in Fig. 6. In Fig. 7, we expand the spectra into the layers. Comparing with Fig. 4, we see an effect of $-0.02\mu_B$ on the spectrum for the second layer C(2). We note that the inclusion of the small Cu moment lifts off the shoulder in the high-energy flank of the main peak that is present in the curve for nonmagnetic Cu (Fig. 6). This slightly improves the agreement of the calculated mean spectrum with the experiment.

We show in Fig. 8 the Co *K*-edge XMCD spectra calculated for the Co/Cu(100) and Co/Cu(111) models. These show slightly greater and shifted main peaks as compared with the experimental spectrum. The broad positive peak observed in the energy range of $10 \leqslant E-E_0 \leqslant 30$ eV is poorly reproduced by the multiple-scattering calculation. We will come back to this point in a later section of this paper.

Up to this point, we have assumed an ideally flat, smooth Co/Cu interface. To illustrate the extent to which the inter-

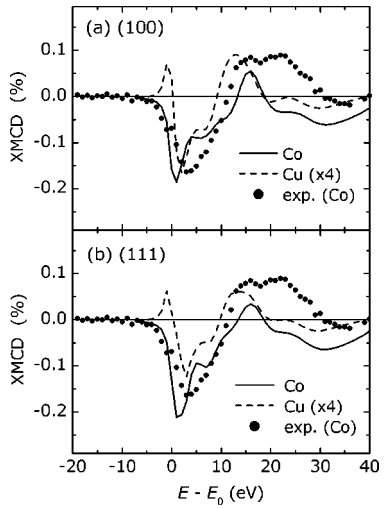

FIG. 8. Mean Co and Cu *K*-edge XMCD spectra for the Co/Cu(100) (a) and Co/Cu(111) (b) models, calculated using the multiple-scattering formalism. The experimental Co spectrum is indicated by dots. The Cu spectrum is multiplied by 4.

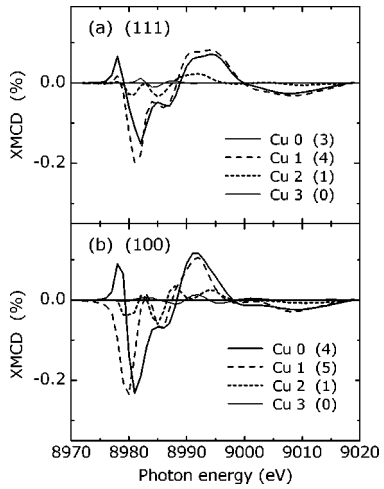

FIG. 9. Single-atom Cu *K*-edge XMCD spectra calculated for Cu atoms labeled 0, 1, 2, and 3 in Fig. 10. Figures in parentheses show the numbers of Co atoms in the nearest-neighbor sites. (a): the Co/Cu(111) model, (b): the Co/Cu(100) model.

face structure can affect the Cu dichroism, and to demonstrate the power of the multiple-scattering calculation at the same time, we show in Fig. 9 single-atom *K*-edge XMCD spectra calculated for nonmagnetic Cu atoms labeled 0, 1, 2, and 3 in Fig. 10. This structure models a hypothetical rough Co/Cu(111) interface. The model assumes parallel straight interface lines passing near atom 0 in the (111) layers above and below the plane of Fig. 10. Note that Cu atoms 0, 1, 2, and 3 have three, four, one, and zero Co atoms in the nearest-neighbor sites, respectively, as indicated in Fig. 9. For reasons of simplicity, the interstitial potential E_i and Fermi energy for atoms 1, 2, and 3 were assumed to be equal to those for atom 0. Figure 9 includes the XMCD spectra calculated for the same types of interface atoms in the Co/Cu(100) model. The Cu XMCD signals approximately scale to the number of Co neighbors, providing more evidence for the

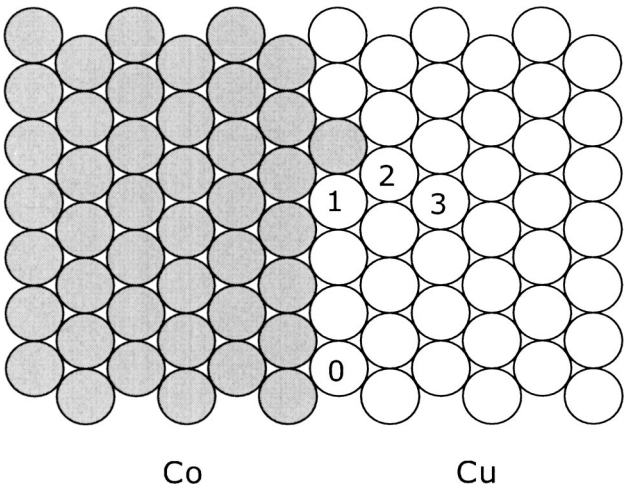

FIG. 10. Model rough Co/Cu(111) interface with a Cu atom substituted by a Co atom. In the (111) planes above and below the plane of the drawing, straight parallel interface lines pass close to Cu 0.

spin-dependent scattering of photoelectrons by nearby Co atoms. Interestingly, the positive peak at ~8978 eV is only observed on atom 0. In view of the similar positive features in Figs. 4 and 5 it is likely that the simple flat, smooth interface is a good approximation of the real mean interface. Combining the multiple-scattering formalism with a statistical model of rough interface would allow us to study more realistic interfaces.[31] Note that the multiple-scattering calculation in real space can handle non-periodic structures, which is not easily feasible by other approaches.[37–39]

V. DISCUSSION

The multiple-scattering approach has successfully explained the *K*-edge XMCD spectra from ferromagnetic 3*d* transition metals and alloys including Fe (Ref. 20–23) and Co (Ref. 25). At these edges, the atomic contribution due to the $\Delta\mu_a$ term [Eq. (8)] occupies a sizable part of the total dichroism.[22,25] This is contrasted to the dichroism of "nonmagnetic" Cu, to which $\Delta\mu_a$ contributes none or very little. The present work confirms this, suggesting that the most part of the *K*-edge XMCD signals observed from "nonmagnetic" metals sandwiched between ferromagnetic metals is accounted for by the spin-dependent scattering of photoelectrons by interface magnetic atoms.

We demonstrated in Fig. 6 that small moments possibly induced on Cu make marginal contributions to the total dichroism. We assumed a $4s+4p$ moment of $-0.02\mu_B$ on all Cu atoms. In practice, this is equivalent to $-0.02\mu_B$ induced only on the interfacial Cu, because the inner layers make insignificant contributions to the total dichroism (Fig. 7). The assumed moment is very close to $-0.023\mu_B$ given by Wu and Freeman to the interfacial Cu sites in their full-potential LAPW calculation[40] and larger than the values ($\sim -0.01\ \mu_B$) presented in the Niklasson *et al.* first-principles Green's function calculation based on the linear-muffin-tin orbital.[41] In a more realistic simulation, we have to include the spin and orbital moments of the *d* state, for which Wu and Freeman give $+0.073\mu_B$.[40] This is much larger than reported by Samant *et al.*.[15] In any case, we emphasize that induced Cu moments would only account for a small fraction of the dichroism observed from Co/Cu multilayers at the Cu *K* edge.

It is worthwhile to point out that if we compress the Co XMCD spectrum along the energy axis towards the absorption edge, the near-edge portion of the Cu spectrum is nearly reproduced except the prepeak at $E-E_0 \approx 0$ (Fig. 2). This can be taken to suggest an incomplete screening of the core holes by $s+p$ electrons in Cu where the *d* electrons are quenched.[42] Core holes in Co would be more efficiently screened by *d* electrons. The incomplete screening pulls down the $s+p$ band of Cu because of the enhanced Coulomb attraction, leading to a compressed XMCD profile.

Our multiple-scattering calculation has reproduced well the observed Cu XMCD spectrum, including the sharp positive feature at $E-E_0 \approx 0$. The Co spectrum is less satisfactorily explained. In particular, the calculation shows a positive peak at ~15 eV above E_0, whereas the observed profile exhibits a much larger feature amounting to two-thirds the

main peak, encompassing the wide range of $10 \leqslant E-E_0 \leqslant 30$ eV. The Co/Cu(100) model gives a slightly better result in this regard (Fig. 8). A similar disagreement is seen in the calculation by Rueff *et al.*,[25] which they ascribe to the unresolved oscillations in the experimental spectrum. In view of the resolution achieved in Fig. 2, we believe that there are no such oscillations as calculated by Rueff *et al.* in the experimental Co spectrum. We note that photoelectrons have a minimal mean free path in this energy range because of the plasmon scattering and others, leading to a significant energy loss due to the many-body effects, which are not included in the present multiple-scattering calculation.

The physical origin of the positive prepeak at $E-E_0 \approx 0$ in the Cu XMCD spectrum is yet to be understood. A similar peak has been observed in the *K*-edge spectra of Fe, but not of Co and Ni. Actually, our Cu spectrum has a profile very similar to the Fe spectrum with a more enhanced prepeak at $E-E_0 \approx 0$. The simple atomic model of XMCD ascribes the Fe prepeak to the density of empty states above the Fermi energy in the majority band, which are occupied in Co and Ni. A possible cause of the Cu prepeak is the local distortion of the $s+p$ band associated with the core holes.[42] In this connection, it is of interest to note a small shoulder at $E-E_0 \approx 0$ in the Co spectrum (Figs. 2 and 8), which can be related to the distorted *d* band. Brouder *et al.*[22] ascribe the prepeak in Fe to the scattering of photoelectrons by the spin-polarized *d* states of the neighboring ions. We may explain the Cu peak in similar terms, referring to the multiple scattering of Cu photoelectrons by the interface Co atoms.

The suppression and cutoff procedures described in Sec. IV imply two Fermi energies for the sample, E_i+10 eV for Co and E_i+9 eV for Cu. This is of course impossible in an equilibrium state, but the local distortion of the conduction electrons in Co and Cu would not instantaneously follow the core-hole potential. In this inequilibrium state the two metals in contact could have unequal Fermi energies. A more sophisticated crystal-potential calculation should take the core holes into account along with the screening.

Finally, we comment on the spin asymmetry of itinerant Cu electrons, which is a key factor in the indirect exchange coupling of Co/Cu multilayers. The *K*-edge XMCD signal cannot be taken as a direct measure of the spin asymmetry because dichroic absorptions are the interplay of the spin asymmetry and the spin-orbit interaction. In the atomic approach, information on the precise relationship between the dichroism signal and spin-polarized densities of states is required to estimate the spin asymmetry. We wonder how multiple-scattering calculations allow us to determine the spin asymmetry from XMCD data. One may estimate the spin asymmetry of delocalized electrons according to the quantum-interference calculation[1] or the Ruderman-Kittel-Kasuya-Yosida (RKKY) model adapted to planar geometries,[43,44] but cannot calculate the dichroism since the spin-orbit coupling is not included in these approaches, at least in the present forms.

ACKNOWLEDGMENTS

We thank N. Hosoito for his cooperation in the XMCD measurement at SPring-8 under proposals No. 2002B0068, No. 2002B0462, and No. 2003A0480. H.H. thanks E. Tamura for discussion. This work is supported by Grant-in-Aid No. 13640318 provided to T. F. by the Ministry of Education, Culture, Sports, Science and Technology.

*Author to whom correspondence should be addressed. Electronic address: hhashizu@ms.naist.jp

[1] P. Bruno, Phys. Rev. B **52**, 411 (1995).
[2] For review see F. J. Himpsel, J. E. Ortega, G. J. Mankey, and R. F. Willis, Adv. Phys. **47**, 511 (1998).
[3] S. S. P. Parkin, Phys. Rev. Lett. **67**, 3598 (1991).
[4] S. S. P. Parkin, R. Bhadra, and K. P. Roche, Phys. Rev. Lett. **66**, 2152 (1991).
[5] M. T. Johnson, S. T. Purcell, N. W. McGee, R. Coehoorn, J. aan de Stegge, and W. Hoving, Phys. Rev. Lett. **68**, 2688 (1992).
[6] P. J. H. Bloemen, R. van Dalen, W. J. M. de Jonge, M. T. Johnson, and J. aan de Stegge, J. Appl. Phys. **73**, 5972 (1993).
[7] N. B. Brookes, Y. Chang, and P. D. Johnson, Phys. Rev. Lett. **67**, 354 (1991).
[8] K. Garrison, Y. Chang, and P. D. Johnson, Phys. Rev. Lett. **71**, 2801 (1993).
[9] C. Carbone, E. Vesscovo, O. Rader, W. Gudat, and W. Eberhardt, Phys. Rev. Lett. **71**, 2805 (1993).
[10] J. E. Ortega and F. J. Himpsel, Phys. Rev. Lett. **69**, 844 (1992).
[11] J. E. Ortega, F. J. Himpsel, C. J. Mankey, and R. F. Willis, Phys. Rev. B **47**, 1540 (1993).
[12] R. Klässges, D. Schmitz, C. Carbone, W. Eberhardt, P. Lang, R. Zeller, and P. H. Dederiches, Phys. Rev. B **57**, R696 (1998).
[13] R. K. Kawakami, E. Rotenberg, E. J. Escocia-Aparicio, H. J. Choi, J. H. Wolfe, N. V. Smith, and Z. Q. Qiu, Phys. Rev. Lett. **82**, 4098 (1999).
[14] For review see Z. Q. Qiu and N. V. Smith, J. Phys.: Condens. Matter **14**, R169 (2002); M. Milun, P. Pervan, and D. P. Woodruff, Rep. Prog. Phys. **65**, 99 (2002).
[15] M. G. Samant, J. Stöhr, S. S. P. Parkin, G. A. Held, B. D. Hermsmeier, F. Herman, M. van Shilfgaarde, L. C. Duda, D. C. Mancini, N. Wassdahl, and R. Nakajima, Phys. Rev. Lett. **72**, 1112 (1994).
[16] S. Pizzini, A. Fontaine, C. Giorgetti, E. Dartyge, J-F. Bobo, M. Piecuch, and F. Baudelet, Phys. Rev. Lett. **74**, 1470 (1995).
[17] I. Yamamoto, S. Nagamatsu, T. Nakamura, T. Fujikawa, and S. Nanao, J. Electron Spectrosc. Relat. Phenom. **125**, 89 (2002).
[18] K. Okamoto, S. Nagamatsu, E. Voronina, T. Fujikawa, and T. Miyanaga, Phys. Scr. (to be published).
[19] K. Okamoto, S. Nagamatsu, E. Voronina, T. Fujikawa, and T. Miyanaga, J. Electron Spectrosc. Relat. Phenom. **141**, 5 (2004).
[20] T. Fujikawa and S. Nagamatsu, Jpn. J. Appl. Phys., Part 1 **41**, 2005 (2002).
[21] T. Fujikawa and S. Nagamatsu, J. Electron Spectrosc. Relat. Phenom. **129**, 55 (2003).
[22] Ch. Brouder, M. Alouani, and K. H. Bennemann, Phys. Rev. B

54, 7334 (1996).
[23] A. Ankudinov and J. J. Rehr, Phys. Rev. B **56**, R1712 (1997).
[24] T. Miyanaga, T. Okazaki, R. Maruko, K. Takagahara, S. Nagamatsu, T. Fujikawa, H. Kon, and Y. Sakisaka, J. Synchrotron Radiat. **10**, 113 (2003).
[25] J. P. Rueff, M. Galéra, Ch. Giorgetti, E. Dartyge, Ch. Brouder, and M. Alouani, Phys. Rev. B **58**, 12 271 (1998).
[26] In a more precise picture, photoelectrons dipole excited to the *p* states at the x-ray absorbing atom sites have their angular momenta coupled with their spins. They are spin-dependently scattered by the exchange potentials of nearby magnetic atoms. The electrostatic potentials of nearby atoms scatter photoelectrons as well, but this is spin independent. The x-ray absorbing atom participates in the chain of multiple scattering through its potential. The magnetic moment on the x-ray absorbing atom contributes to $\Delta\mu_n$ as well as to $\Delta\mu_a$. We confirm that the spin-orbit interactions additionally induced on photoelectrons at neighboring atom sites marginally affect $\Delta\mu_n$ (Ref. 20).
[27] G. Parratt, Phys. Rev. **95**, 359 (1954).
[28] M. Suzuki, N. Kawamura, M. Mizumaki, A. Urata, H. Maruyama, S. Goto, and T. Ishikawa, Jpn. J. Appl. Phys., Part 2 **37**, L1488 (1998).
[29] M. Suzuki, N. Kawamura, and T. Ishikawa, Proc. SPIE **4145**, 140 (2001).
[30] N. Ishimatsu, H. Hashizume, S. Hamada, N. Hosoito, C. S. Nelson, C. T. Venkataraman, G. Srajer, and J. C. Lang, Phys. Rev. B **60**, 9596 (1999).
[31] C. S. Nelson, G. Srajer, J. C. Lang, C. T. Venkataraman, S. K. Sinha, H. Hashizume, N. Ishimatsu, and N. Hosoito, Phys. Rev. B **60**, 12 234 (1999).
[32] N. Hosoito, H. Hashizume, N. Ishimatsu, I-T. Bae, G. Srajer, J. C. Lang, C. K. Venkataraman, and C. S. Nelson, Jpn. J. Appl. Phys., Part 1 **41**, 1331 (2002).
[33] Y. Hayasaki, K. Ishiji, H. Hashizume, N. Hosoito, K. Omote, M. Kuribayashi, G. Srajer, J. C. Lang, and D. Haskel, J. Phys.: Condens. Matter **16**, 1915 (2004).
[34] A. L. Ankudinov, B. Ravel, J. J. Rehr, and S. D. Conradson, Phys. Rev. B **58**, 7565 (1998).
[35] P. Zahn, J. Binder, I. Mertig, R. Zeller, and P. H. Dederichs, Phys. Rev. Lett. **80**, 4309 (1997).
[36] M. O. Krause and J. H. Oliver, J. Phys. Chem. Ref. Data **8**, 329 (1979).
[37] H. Ebert, Rep. Prog. Phys. **59**, 1665 (1996).
[38] N. V. Smith, C. T. Chen, F. Sette, and L. F. Mattheiss, Phys. Rev. B **46**, 1023 (1992).
[39] K. Hirai, Physica B **345**, 209 (2004).
[40] R. Wu and A. J. Freeman, J. Appl. Phys. **79**, 6500 (1996).
[41] A. M. N. Niklasson, B. Johansson, and H. L. Skriver, Phys. Rev. B **59**, 6373 (1999).
[42] E. Tamura (private communication).
[43] Y. Yafet, Phys. Rev. B **36**, 3984 (1987).
[44] Y. Yafet, J. Kwo, M. Hong, C. F. Majkrzak, and T. O'Brien, J. Appl. Phys. **63**, 3453 (1988).